Modeling InSAR Phase and SAR Intensity Changes Induced by Soil Moisture

Yusuf Eshqi Molan and Zhong Lu, *Senior Member, IEEE*

***Abstract*— A broad range of studies have been conducted so far to quantify the effect of soil moisture on synthetic aperture radar (SAR) intensity and interferometric synthetic aperture radar (InSAR) phase. The introduced models are either intensity or interferometric models, and there is no single scattering model that can estimate both intensity and phase changes, indicating the subject is poorly understood. Here, we quantify the influence of soil moisture on InSAR phase and SAR intensity by employing a volume scattering model. We model soil as a collection of randomly distributed independent point scatterers embedded in a homogeneous background. Our volume scattering model successfully estimates SAR intensity and InSAR phase changes due to soil moisture changes. In addition to soil moisture changes, the model also takes into account the scatterers' size and their volumetric fraction. This may open a new window in the study of soil structure using SAR images and InSAR methods. Our results indicate that the structure of soil manipulates the way soil moisture alters the SAR intensity and InSAR phase. The model has been evaluated against field soil moisture measurements and shown to be successful in modeling InSAR phase and SAR intensity.**

***Index Terms*— Interferometric synthetic aperture radar (InSAR) phase, modeling, synthetic aperture radar (SAR) intensity, soil moisture.**

I. Introduction

INTERFEROMETRIC synthetic aperture radar (InSAR), which is an all-weather, day-or-night technique, has the ability to remotely sense millimeter to centimeter scale surface deformation with a high spatial resolution of tens of meters or better [1]–[3]. InSAR provides valuable input to the study of earthquakes, volcanos, landslides, permafrost processes, and so on [3]–[5]. Two synthetic aperture radar (SAR) images taken at different times are combined to make an interferogram to detect ground surface deformations as well as to generate digital elevation models (DEMs) [1]–[3]. Between the two images, the water content of the soil being imaged is subject to change. The temporal change in soil moisture has been known to contribute to InSAR phase and SAR intensity changes [6]–[10]. Consequently, InSAR-detected ground displacement can be systematically biased by the changes in soil moisture. The uncompensated biases in the spatial and temporal patterns of InSAR detected-displacement limit the reliability and robustness of InSAR [6]–[10].

Unlike ground deformations, which are spatially and temporally correlated, the spatial and temporal variabilities of soil moisture are complex [11], and in practice, the influence on InSAR phases can be confused with atmosphere artifacts. Some atmospheric artifacts can be compensated by utilizing spatial–temporal filters [11], [12] since they often feature spatially correlated variations [13]. Unlikely, soil moisture is not always correlated spatially as its value varies abruptly, for example, across boundaries of two agricultural fields or different land cover types [11]–[14]. Soil moisture's temporal variability is also intricate [11]–[14]. Therefore, temporal filters may not be as practical as it is to mitigate turbulent tropospheric phase artifacts, which are temporally uncorrelated on time scale of days [13]. Also, in some cases, terrestrial processes and subsequent movements are closely related to the changes in soil moisture. For example, sudden landslides can happen after rapid snowmelt or heavy precipitation [15]. Soil moisture also indicates groundwater conditions [16] and is in a close relationship with permafrost thawing and deformation [4]. Broadly speaking, soil moisture is a key variable in agricultural and environmental studies [17]–[19] and plays a vital role in the terrestrial water cycle, exchange of energy and carbon fluxes between the atmosphere and the land surface [18], [19].

Potentially, modeling soil moisture influence on InSAR phase measurements and SAR intensity changes provides a means to compensate soil moisture-induced InSAR phase artifacts and also to retrieve surface soil moisture. The first reported signal of soil moisture on InSAR images has been reported in [14]. One of the interferograms over the agricultural field in California, generated using SEASAT data, featured phase changes corresponded to field boundaries. The observed phase was inferred to be related to soil moisture. Swelling characteristics of the soil convinced the authors to ascribe the phase change to surface movement (expansion), i.e., shortening in the travel path of radar wave. Since then, soil moisture-induced phase changes on interferograms from satellite SAR data [7], [8], [20], and airborne and indoor experiments [21]–[23] have been continued to be reported.

New experimental studies later cast doubt on the expansion hypothesis. For instance, Rudant *et al.* [24] in a laboratory experiment noted apparent subsidence over wetted soil and sprinkled planets. Hensley *et al.* [11] and Morrison *et al.* [25] also noticed that the phase change is larger than the deformation of the surface of the soil, indicating that the observed phase cannot be caused by a realistic deformation.

Manuscript received October 17, 2019; revised January 21, 2020; accepted January 27, 2020. This work was supported in part by the NASA Earth Surface and Interior Program under Grant 80NSSC19K1491 and Grant NNX16AK56G and in part by the Shuler-Foscue Endowment at Southern Methodist University. *(Corresponding author: Yusuf Eshqi Molan.)*

The authors are with the Department of Earth Sciences, Southern Methodist University, Dallas, TX 75205 USA (e-mail: yeshqimolan@smu.edu; yusuf.molan@gmail.com; zhonglu@smu.edu).

Color versions of one or more of the figures in this article are available online at http://ieeexplore.ieee.org.

Digital Object Identifier 10.1109/TGRS.2020.2970841

Alternatively, the influence of soil moisture on the InSAR phase has been attributed to soil volume scattering [9], [10]. Zwieback *et al.* [9] empirically analyzed the applicability of the aforementioned hypotheses. Using the data of two L-band airborne campaigns, the authors revealed that the soil moisture-induced phase was not consistent with the penetration depth or the soil swelling hypotheses but only with dielectric volume scattering mechanism. Upon wetting, the dielectric constant of the soil and consequently the optical path between the antenna and the scatterers in the soil volume increase. As the soil absorbs water, the replacement of air within free spaces of soil by water increases the dielectric constant of the soil since the magnitude of the dielectric constant of water is much greater than that of air or sand grains. The increase in dielectric constant corresponds to an increase in the wavenumber in the soil, which gives rise to an increase in phase. This is manifested as a movement away from the antenna or an apparent subsidence of the surface, even with no mechanical deformation on the ground.

So far, a broad range of studies from controlled experiments to observational studies without soil moisture information have been conducted to quantify the effect of soil moisture on SAR intensity and InSAR phase and coherence [4], [6]–[10], [7], [8], [11], [14], [20]–[26]. The models can be divided into interferometric and intensity models. On the one hand, a number of interferometric models have provided mathematical volume scattering models ranging from simple analytical expression (see [9]) to more complicated numerical solutions to Maxwell's equations to estimate soil moisture-induced InSAR phase artifacts (see [10]). Basically, the models can potentially be used or modified for different soil types as well as layered and/or depth-resolved observations. However, all the interferometric models that share in common is that the temporal change in volume soil moisture has been purported to be the primary influential factor in the models. Hence, these interferometric models do not consider the influence of soil's structure, i.e., the size and distribution of scatterers, on InSAR phase changes. On the other hand, intensity models usually attribute soil moisture-induced SAR intensity changes to surface scattering solely [27]–[31], and volume scattering is either neglected or employed along with surface scattering models to provide an explanation for negative slope that appears on SAR intensity curves at small soil moisture values [32], [33].

To the best of our knowledge, no volumetric soil moisture model has been introduced that takes into account the soil volumetric structure and addresses both intensity and phase changes. In this article, we present a new approach and a comprehensive model to estimate soil moisture-induced SAR intensity and InSAR phase changes. To this end, we model the soil as a collection of discrete coarse scatterers, i.e., with a diameter of few centimeters or larger, embedded in an attenuating dielectric medium comprising of finer soil grains. Therefore, our volume scattering model can not only provide an improved estimation of soil moisture-induced intensity and phase changes but also potentially be used to infer soil structure. The rest of this article is structured as follows: Section II describes the introduced volume scattering model. Section III includes simulated results. Section IV provides a discussion on the results and also mathematical analyses to support the outcomes. Section V provides validation of results. Conclusions appear in Section VI.

II. Volume Backscattering Model

Here, we model the expected return signal from a pixel after SAR focus. Soil, the scattering object, is modeled as a half-space dielectric medium with N randomly distributed independent point scatterers in a resolution cell. When an electromagnetic wave strikes on the soil surface, a part of the incident wave reflects away, whereas a fraction of it transmits into the soil and decays exponentially at a rate governed by the imaginary part of the medium's complex wavenumber [34]–[36]. Also, as the wave propagates through the medium, its phase is manipulated by the real part of the medium's complex wavenumber [34]–[36]. Once the wave is scattered by a point scatterer within the soil medium, a part of the scattered wave propagates backward. Through the backward propagation, the dielectric medium again modifies its amplitude and phase until it reaches the soil–air boundary. A part of the transmitted wave at the soil–air interface propagates back toward the antenna. Then, the signal is further modified by applying slant range and azimuth resolution functions, W_a and W_r, respectively. Finally, the scattered signal from a single scatterer located at (x_i, y_i, z_i) within the soil becomes

$$u_i = e^{j2kR} t_{1,2} t_{2,1} s_i e^{\frac{2\alpha z_i}{\cos(\theta_r)}} \times e^{j2(k_0 y_i \sin(\theta_r) + \beta z_i \cos(\theta_r)) W_a(x_i) W_r(y_i \sin(\theta_r) n \cos(\theta_r) z_i)} \quad (1)$$

where n is the refraction index of the medium, θ_i and θ_r are the incident and refracted angles, respectively, $t_{i,j}$ is the one-way transmission coefficient of amplitude from medium i to medium j, R is the propagation distance, i.e., the slant range of the pixel, α and β are real and imaginary parts of $j\gamma$, which γ, α, and β are propagation, absorption, and phase constants of the medium, k_0 is the free air wavenumber, and s_i is the scattering amplitude of the scatterer.

The complex-valued SAR backscattering $\boldsymbol{u}$, i.e., the total backscattering from the scattering points within a resolution element, is the coherent summation of the point scatterers' backscattering [37], [38]

$$\boldsymbol{u} = \sum_{i=1}^{N} u_i \quad (2)$$

where u_i is the backscattering signal of the point scatterer located at (x_i, y_i, z_i) within the soil. The point scatterers are randomly distributed in the soil volume, randomizing the total signal which is the summation of random signals. By assuming uniform random distribution, the soil volume can be considered as a symmetric target in the azimuth and ground range directions, meaning that the backscattered signal is a function of variations in the vertical direction.

The pixel's backscattering is the collection of contributions of all scatterers (grains) embedded in the soil [38]. The scattering and absorption coefficients of a scatterer are functions of its size, dielectric constant, and the wavelength. In the cases where the particle size is much smaller than the

wavelength, i.e., clay, silt, and sand soil particles, Rayleigh approximation can be used to express the scattering, extinction, and absorption coefficients [34]–[36]. It is an approximation of Mie equations and can be expressed only by the first two terms of the Mie series [35], [36]

$$\xi_s = \frac{8}{3}\chi^4|K|^2 \tag{3}$$

$$\xi_e = \chi \mathrm{Im}(-K) + \frac{8}{3}\chi^4|K|^2 \tag{4}$$

$$\xi_a = \xi_e - \xi_s \tag{5}$$

where ξ_s, ξ_e, and ξ_b, are the scattering, extinction, and backscattering efficiencies, respectively, and

$$-K = \frac{n^2 1}{n^2+2} \tag{6}$$

$$\chi = \frac{2\pi r_p}{\lambda}\sqrt{\epsilon'_b} \tag{7}$$

$$n = \frac{n_p}{n_b}. \tag{8}$$

In the above equations, λ is the free space wavenumber, r_p is the radius of the point scatterer, ϵ'_b is the real part of the dielectric constant of the background, n_p and n_b are complex indices of refraction of the scatterer and the background, and n is the ratio of the two refraction indices.

The expressions in (2) are valid only for $|n\chi| \ll 0.5$ [34], [35]. Consequently, for L-band radar measurements, the Rayleigh approximation is always valid for medium and small grains, i.e., sand, silt, and clay, even with large dielectric constants of the soil. For larger grain sizes, e.g., gravel, depending on the dielectric constant, the assumption may not always be satisfied. Once the dielectric constant of the soil increases, the indicator $|n\chi|$ gradually increases to reach values larger than 0.5 [see (6) and (7)]. For C-band measurements, depending on the dielectric constant of the medium, the Rayleigh approximation may not be applicable even for medium grain sizes. In such cases, Mie equations [35], [39], [40], which involve no approximations, should be used instead.

Using Mie solutions, the scattering, extinction, and backscattering efficiencies and scattered complex amplitudes are expressed in the form of converging series [35], [39], [40]

$$\xi_s = \frac{2}{\chi^2}\sum_{k=1}^{\infty}(2k+1)(|a_k|^2+|b_k|^2) \tag{9}$$

$$\xi_e = \frac{2}{\chi^2}\sum_{k=1}^{\infty}(2k+1)\mathrm{Re}(a_k+b_k) \tag{10}$$

$$\xi_b = \frac{1}{\chi^2}|\sum_{k=1}^{\infty}(2k+1)(1)^k(a_k b_k)|^2 \tag{11}$$

$$S_{1(\cos\theta)} = \sum_{k=1}^{\infty}\frac{2k+1}{k(k+1)}(a_k\pi_k + b_k\tau_k) \tag{12}$$

$$S_{2(\cos\theta)} = \sum_{k=1}^{\infty}\frac{2k+1}{k(k+1)}(a_k\tau_k + b_k\pi_k) \tag{13}$$

where S_1 and S_2 are the scattered complex amplitudes for perpendicular and parallel polarized waves, respectively. In the above equation, θ is the scattering angle, π_k and τ_k are the functions of θ and n, and finally a_k and b_k are known as the Mie coefficients. The equations for the coefficients are not repeated here, instead interested readers are referred to [35], [39], [40] and the references therein for more details about the coefficients and strategies to calculate them.

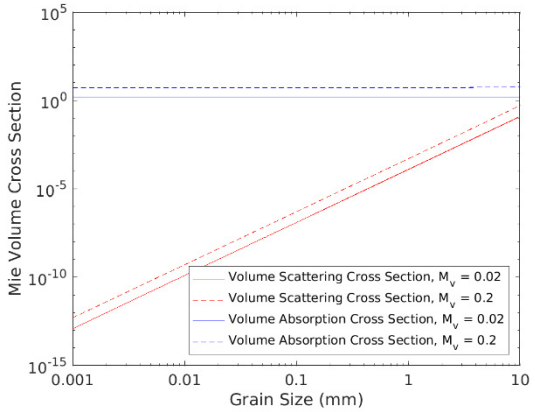

Fig. 1. Mie volume scattering and absorption cross sections for different grain sizes.

Once the Mie efficiencies are calculated, the volume cross sections (m^2/m^3) are obtained by summing cross sections (m^2) over N_v ($-m^3$) particles per unit volume

$$\kappa_s = \sum_{k=1}^{N_v} Q_s(r_k) = \sum_{k=1}^{N_v}\xi_s(r_k)\times\pi r_k^2 \tag{14}$$

$$\kappa_e = \sum_{k=1}^{N_v} Q_e(r_k) = \sum_{k=1}^{N_v}\xi_e(r_k)\times\pi r_k^2 \tag{15}$$

where κ_s and κ_e are volume scattering cross section and volume extinction cross section, respectively, and N_v is the number of point scatterers embedded in the soil. The volume absorption coefficient is related to the absorption constant of the medium α by $\kappa_a = 2\alpha$ [35]. The extinction coefficient κ_e includes the scattering coefficient κ_s and absorption coefficient κ_a of dielectric medium [32], [41], [42]

$$k_e = k_s + k_a. \tag{16}$$

Fig. 1 shows the plot of Mie volume scattering and volume extinction cross sections [see (14) and (15)] for different grain sizes. It can be seen that the Mie volume scattering cross section, plotted in logarithmic coordinates in Fig. 1, increases by enlarging the size of grains. For example, the Mie volume scattering cross section of a grain with a size of 10 mm is about 1000 times larger than that of a grain with a size of 1 mm (Fig. 1). This means that the scattering of gravel grains with a radius of 1 cm occupying only 1% of a soil's solid volume is ten times larger than the scattering of background grains with grain size of 1 mm occupying 99% of the total solid volume.

Unlike the volume scattering cross section, the volume extinction function is almost independent of grain size, at least for the range of sizes we study in this article, i.e., up to a few centimeters. This means that the signal scattered by the soil volume is dominated by larger grains and that the contribution of smaller grains becomes negligible if large grains exist in

the soil. However, all grains, regardless of their size, equally contribute to the absorption.

III. Simulating Results

A. Constant Soil Moisture Profile

Here, we provide simulation results for soils with different structures and soil moisture changes. In our model, the soil volume is assumed to a collection of randomly distributed point scatterers, i.e., larger grains, and embedded in a lossy dielectric medium, i.e., finer grains. Without loss of generality, we assume a soil with $\bar{N}_v$ point scatterers of the same size r_p occupying f_s percent of the soil's total volume

$$\bar{N}_v = \frac{3f_s}{4\pi r_p^3} \tag{17}$$

where f_s is the fraction of the total volume occupied by the scattering soil particles. Then, we calculate soil moisture-induced interferometric phase and SAR intensity changes over the soil with different r_p and f_s values. The dielectric constant of the wet soil was calculated using Hallikainen mixing model [43]. By increasing soil moisture, water fills the free spaces between the particles in the porous background. This increases the dielectric constant of the background. Unlike the porous background, large grains can only be wrapped by a layer of water. The thickness of the water layer increases by increasing soil moisture, and its maximum thickness is related to the size of the free spaces, i.e., voids between background grains. To estimate the dielectric constant of a grain wrapped by a layer of water, we used Maxwell–Garnett [44] mixing equation [45]

$$\varepsilon_{\text{eff}} = \varepsilon_0 + 3f\varepsilon_0 \frac{\varepsilon_s \varepsilon_0}{\varepsilon_s + 2\varepsilon_0 f(\varepsilon_s \varepsilon_0)} \tag{18}$$

where $f = (v_s)/(v_s + v_l)$ is the volume fraction of the solid grain, ε_{eff} is the effective dielectric constant, ε_0 is the dielectric constant of water, ε_s is the dielectric constant of the grain, v_s is the volume of the grain, and v_l is the value of the water layer. It should be noted that unlike the dielectric constant of the background, the dielectric constant of the larger grains, i.e., scatterers, slightly increases because the thickness of the water layer, which is related to the dimension of the free spaces, is much smaller than the size of scatterers.

Fig. 2 shows the modeled interferometric phase and intensity changes for different soil types as a function of r_p and f_s [see (1) and (2)]. It can be seen that the intensity is proportional to the volume geometric cross section, i.e., $\sigma_g = \pi r_p^2 \bar{N}_v$, whereas the phase change is proportional to $1/\sigma_g$.

B. Variable Soil Moisture Profile

Constant soil moisture profile has been assumed to derive (1). This means that the attenuation and phase constants of the soil are independent of depth. However, with variable soil moisture profiles, the attenuation and phase constants become functions of depth and we can rewrite (1) as

$$\boldsymbol{u} = \sum_{i=1}^{N} e^{j2kR} t_{1,2} t_{2,1} s_i e^{2\int_0^z \frac{\alpha}{\cos(\theta_r)} dz'} e^{j2(k_0 y_i \sin(\theta_r))} e^{2j\int_0^z \beta \cos(\theta_r) dz'} W_a(x_i) W_r(y_i \sin(\theta_r) n \cos(\theta_r) z_i). \tag{19}$$

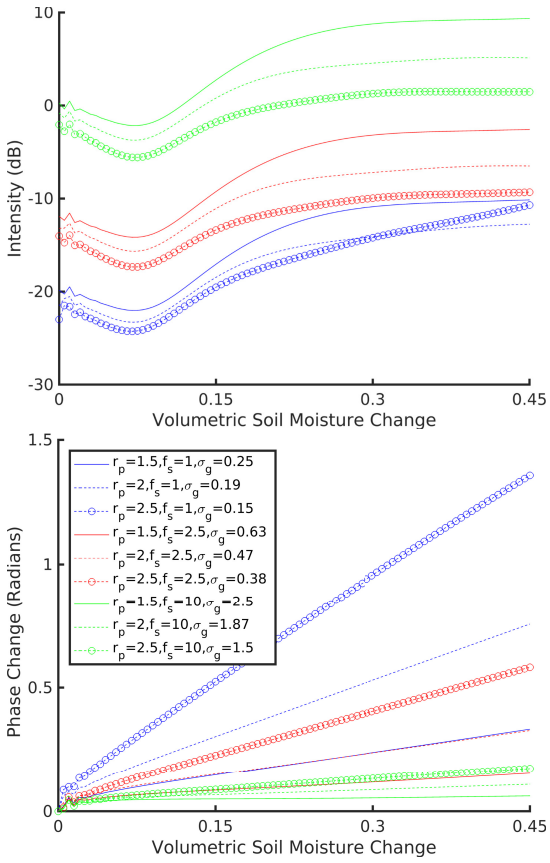

Fig. 2. L-band soil moisture-induced SAR intensity changes and InSAR phase changes for different soil structures and different soil moisture changes.

Fig. 3 shows the modeled SAR intensity and interferometric phase over soil with different soil moisture profiles. The soil is loam containing 1.5% gravel grains of the average radius of 2.5 cm. The soil moisture values at the surface are in the range of 0–0.50 and linearly changes with depth until it becomes 0.40 at depth 40 cm. In order to generate interferometric phases, we assume the master image to have a variable soil moisture profile with a value of 0.10 at surface and 0.40 at the depth 40 cm. The results show that the depth-resolved and depth-averaged backscattered intensities are almost equal when shallow depths hold large soil moisture. Note that depth-resolved means a profile of variable soil moisture whereas depth-averaged indicates a constant soil moisture profile. However, by decreasing the soil moisture values at shallow depths, the depth-averaged intensities take larger values compared to the depth-resolved intensity. Similar results can be seen in phase changes where a larger difference between depth-resolved and depth-averaged phase changes can be observed at smaller soil moisture values.

IV. Discussion

There are two main steps in modeling soil moisture-induced intensity and phase changes of a single-looked pixel on an SAR image. The first step is to model the dielectric medium (soil here) and the second step is to estimate the intensity and phase changes due to changes in soil moisture. Most of the models introduced so far model soil as a continuous scattering medium [9], [10]. The models then use a cross correlation between two soils with different soil moisture

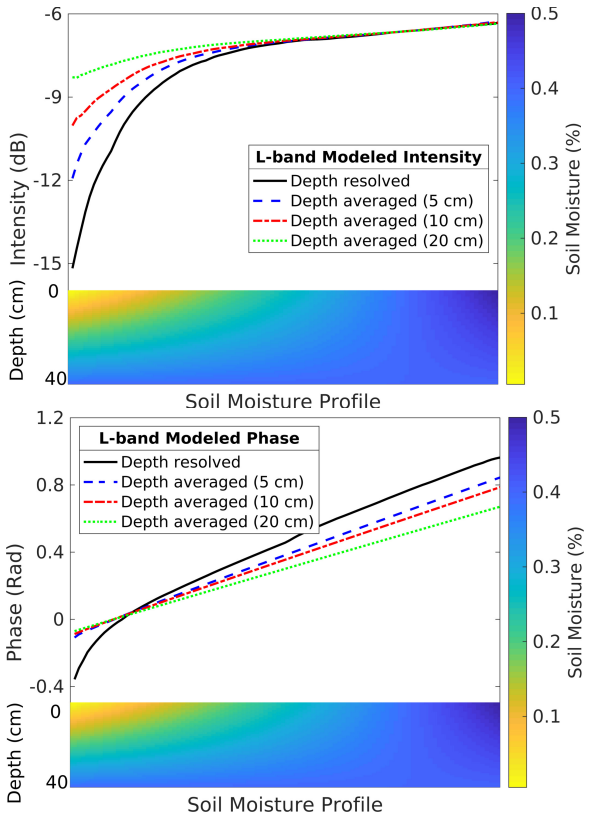

Fig. 3. L-band soil moisture-induced SAR intensity and phase changes for uniform and variable soil moisture profiles.

values to estimate the phase change. The model introduced in this article, however, differs in strategy from the previous models in two ways. The first is that the model in this article considers the soil to be a discrete dielectric medium. The second lies in the approach we used to estimate the soil moisture-induced intensity and phase changes. The previous models aim to model the cross correlation between two single-looked pixels. On the contrary, the model in this article is an SAR-based model that directly quantifies SAR intensity of a single-looked pixel as a function of soil moisture. It also calculates the phase change of an SAR pixel as a function of soil moisture.

A. Modeling Dielectric Medium (Soil)

Generally, there are two main approaches that can be used to model a scattering object in order to estimate the phase and intensity changes. The first approach is to consider the scattering object as a collection of discrete scatterers embedded in a dielectric medium. In this model, the contribution of a single scatterer to the scattered signal is a function of its size, position, and dielectric constant of the scatterer, and the medium's dielectric constant. The second approach is to assume the scattering object as a continuous medium. The total signal in the case of the continuous medium is expressed as a coherent sum of correlation among pairs of infinitesimal slabs along the vertical direction. This mathematically implies that every infinitesimal particle of the entire soil profile acts like a scattering object. The model neglects the influence of the structure of the soil, i.e., the dimensions and distribution of scatterers, on the scattered signal. However, as explained

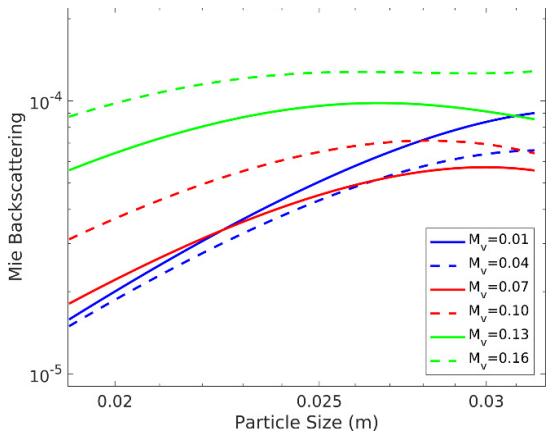

Fig. 4. Mie backscattering for different soil moisture values and different particle sizes. M_v is volumetric soil moisture (ratio of soil volume occupied by water).

in Section II, the backscattering of a scatterer is a function of its size [35]. Fig. 4 shows such a relationship between grain size and Mie scattering cross section. The relationship between a scatterer's size and its backscattering, illustrated in Figs. 1 and 4, indicates that the scatterers' size should be considered in the models. It also indicates that a small grain's contribution to the total signal is negligible compared to the contribution of a larger grain in the models. However, all grains, regardless of their sizes, equally contribute to the absorption. This means that scattering is a function of scatterer size and absorption is independent of it. Therefore, considering these, we have modeled the soil as a collection of discrete coarse scatterers embedded in an attenuating dielectric medium.

B. Estimating Intensity and Phase Changes

Once the dielectric medium, i.e., soil, is modeled as a collection of scatterers, the soil moisture-induced intensity and phase changes can be estimated by exploiting a model. Imagine that n scatterers, i.e., $a_{1,1}e^{j\varphi_{1,1}}, a_{1,2}e^{j\varphi_{1,2}}, \ldots, a_{1,n}e^{j\varphi_{1,n}}$, are within the single-looked pixel $\boldsymbol{u_1}$ on the first image where $a_{1,i}$ and $\varphi_{1,i}$ are the amplitude and phase of the scattered signal of the ith scatterer. Now, imagine that changes happened in soil moisture. This in turn leads to the changes in the amplitudes and phases of the scatterers. Therefore, for the same pixel on the second image, the backscattering values of the scatterers are $a_{2,1}e^{j\varphi_{2,1}}, a_{2,2}e^{j\varphi_{2,2}}, \ldots, a_{2,n}e^{j\varphi_{2,n}}$. Now, a model should be exploited to quantify phase change of the single-looked pixel between the two SAR images due to soil moisture change. The common approach in the literature has been applying a cross correlation between the two scattering objects, i.e., soil here. Therefore, the phase change can be calculated by

$$\emptyset_{1,2} = \arg\left(\sum_{i=1}^{n} a_{1,i}a_{2,i}\frac{e^{j\varphi_{2,i}}}{e^{j\varphi_{1,i}}}\right). \tag{20}$$

Note that SAR images are not generated in this approach and phase change is estimated from two modeled scattering objects by exploiting cross correlation. Cross correlation is a common approach to estimate the interferometric phase in the

multilooking process. However, the performance of cross correlation applied in modeling scattering objects is different from that of cross correlation conducted in multilooking processing aiming to improve phase estimation. In multilooking processing, the single-looked pixels in the multilooking window on the first image are multiplied to the complex conjugate of the equivalent single-looked pixels on the second image. Here, however, cross correlation is conducted between the stable point scatterers within the first single-looked pixel and the point scatterers within the second single-looked pixel. This means that the scatterers within the single-looked pixel on the first image are multiplied to the complex conjugate of the equivalent scatterers on the second image.

We argue here that applying cross correlation to model soil moisture-induced phase changes causes phase artifacts. Since the amplitudes of the equivalent single-looked pixels are multiplied [see (20)] using cross correlation in the multilooking process, weaker pixels, i.e., pixels with smaller amplitude and noises, have less influence on the estimated multilooked phase. Thus, multilooking improves phase estimation by decreasing the influence of weaker pixels. Unlike this, cross correlation, however, can lead to biased phase estimations when it is exploited for dielectric mediums, e.g., soil. Soil is a loosy dielectric medium, and the phase of a scatterer increases by increasing its depth, whereas its amplitude decreases at the same time. In this case, weaker scatterers, i.e., deeper scatterers with smaller amplitudes, are associated with larger phases. This means that by applying cross correlation, scatterers with larger phases have less influence on the estimated phase. Since this effect increases by increasing soil moisture changes, phase curves tend to saturate at higher soil moisture changes. Saturated phase curves have been documented in previous models [9], [10] in which cross correlation has been used to model soil moisture-induced interferometric phase.

Another consequence is the nonzero closure phase for single-looked pixels, which has been documented in the previous models [9], [10]. Note that the closure phase of single-looked pixels is zero in observations. This effect is similar to phase artifact in multilooking process and interested readers are referred to Molan *et al.* [46] for more details about the multilooking artifacts. We also notice that, in practice, unlike the cross-correlation approach, we use SAR images to generate interferograms since the signals of the single point scatterers within the soil volume are not available separately.

In this article, instead of applying cross correlation, we first model SAR pixel and then calculate the phase and intensity changes between SAR images with different soil moisture values. A single pixel on an SAR image is a vector summation of the signals of single scatterers within the resolution cell

$$\boldsymbol{u}_j = \sum_{i=1}^{n} a_{j,i} e^{j\varphi_{j,i}}. \tag{21}$$

Then, the interferometric phase of two single-looked pixels on SAR images is simply calculated by subtracting the phase of the first SAR image from the phase of the second image

$$\emptyset_{1,2} = \varphi_2 \varphi_1 = \arg\left(\frac{\sum_{i=1}^{n} a_{2,i} e^{j\varphi_{2,i}}}{\sum_{i=1}^{n} a_{1,i} e^{j\varphi_{1,i}}}\right). \tag{22}$$

TABLE I
DATE (YYYY-MM-DD) OF THE SLC IMAGES

No.	date	No.	date	No.	date
1	2007-07-05	7	2008-07-07	13	2010-05-28
2	2007-08-20	8	2009-01-07	14	2010-07-13
3	2007-11-20	9	2009-07-10	15	2010-08-28
4	2008-01-05	10	2009-10-10	16	2010-10-13
5	2008-04-06	11	2010-01-10	17	2011-02-28
6	2008-05-22	12	2010-04-12		

Here, one may argue that a shallower scatterer with larger amplitude contributes to an SAR pixel's signal more than a deeper scatterer with smaller amplitude, alike the aforementioned case in cross correlation. However, it should be noted that the influence of amplitude on the interferometric phase between two acquisitions decreases because amplitude appears in the denominator as well as the numerator of the (22). On the other hand, as it can be seen in (20), the counterbalancing of amplitude influence does not happen in cross correlation. Instead, cross correlation increases the influence of the amplitude by multiplying the amplitudes.

C. Negative Slope on SAR Intensity Curves

One of the features, which is occasionally observed on SAR intensity curves, is an inverse relation between soil moisture and backscatter for small soil moisture values, e.g., mv $<$ 0.10. This phenomenon is thought to be due to a decrease in the subsurface scattering and an increase in surface scattering upon wetting [32], [32]. However, not all intensity curves feature such a negative slope for small soil moisture values, indicating that this may not the case. We argue that the negative slope appears when the dielectric constant of the dry background, e.g., silt, sand, and clay, is smaller than the dielectric constant of point scatterers, e.g., gravel-sized grains. The porous background has a smaller dielectric constant compared to the individual larger soil particle due to the smaller dry bulk density. As the background soil absorbs water, its dielectric constant increases and gets closer to the dielectric constant of the point scatterers, resulting in decreased backscatter at their interface. The backscattering then increases upon more wetting. Fig. 4 shows the Mie backscattering [see (11)] of point scatters with a dielectric constant of 3.3 embedded in a background with a dielectric constant of 2.5 at the dry condition. As it can be observed on the plot, backscattering decreases at first and then increases upon more wetting.

V. EVALUATION

To evaluate our model, we choose ALOS PALSAR data over Idaho where *in situ* soil moisture measurements are available at the Orchard Range Soil Climate Analysis Network (SCAN) station (https://www.wcc.nrcs.usda.gov/). Co-registered single-looked complex (SLC) images are used to generate multilooked interferograms with 6 and 3 looks in azimuth and range, respectively. Table I provides the dates of the SAR images. The path and frame numbers are 208 and 860, respectively. The topographic phase is simulated using the DEM of Shuttle Radar Topography Mission (SRTM) with 1 arc-sec spatial resolution and is then removed from the interferograms. After removing those interferograms with low

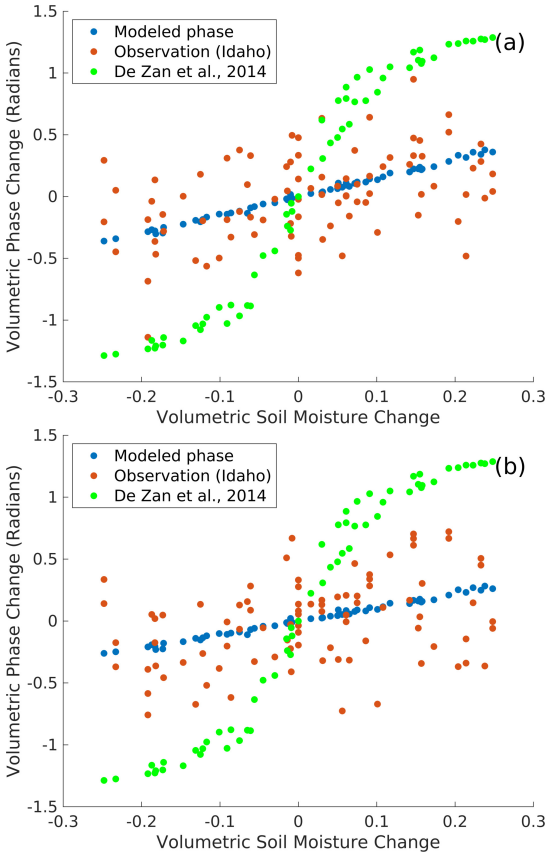

Fig. 5. Modeled and observed interferometric phases at point (a) with a grain size of 2.8 cm and volume fraction of 3.6%, and point (b) with a grain size of 2.75 cm and volume fraction of 5.2%.

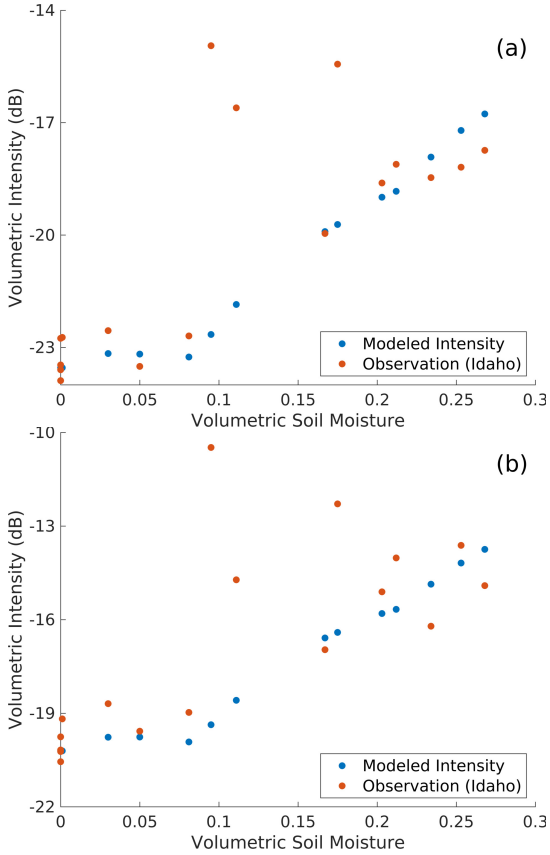

Fig. 6. Modeled and observed SAR intensity.

coherence over the soil moisture station, a total of 87 remaining interferograms are selected. The perpendicular baseline of the selected interferograms ranges between 12 and 1970 m, and the maximum temporal baseline is 1196 days.

Fig. 5 illustrates the comparison between our model and the model introduced by Zan *et al.* [10] with observed interferometric phases at two pixels around the station where soil moisture measurements are available. The model introduced in [10] has been used for soil moisture estimations and later revised by Zwieback *et al.* [33] to accommodate depth variable soil moisture cases. This model assumes the temporal changes in soil moisture to be the primary influential factor. Hence, it does not consider the influence of soil's structure on InSAR phase changes. Therefore, unlike our model, its estimated phase for (a) and (b) cases (see Fig. 5) are the same regardless of their different phase behaviors due to different soil structures. In Fig. 6, the modeled intensity is compared with the observed in tensity at two points (a) and (b). Also, in Fig. 7, modeled intensity changes are compared with observed intensity changes at points (a) and (b). The plots show that our model is very successful in the estimation of InSAR phase and SAR intensity. By fitting the modeled phase and intensity values to the observed intensity and phase values (see Figs. 6 and 7), the grain sizes of 2.8 and 2.75 cm with volume fractions of 3.6% and 5.2%, respectively for (a) and (b) are estimated. The dielectric constant of the scatterers is also estimated to be 2.7, and the maximum layer of water that wraps larger grains is estimated to be 1.1 mm.

Upon wetting, the replacement of air within free spaces of soil by water increases the dielectric constant of the soil. The increase in dielectric constant corresponds to an increase in the wavenumber in the soil. This means that the wavefronts propagating in the soil become closer as the soil becomes wetter. However, soil moisture contribution to the final signal received by antenna appertains more to soil structure. Generally, as the density of scatters increases, the magnitude of scattered waves at shallower depths increases, and relatively smaller portion of the wave has the chance to reach deeper depths and gain larger phase changes. This is because of a wave backscattered by a scatterer at depth 10 cm, for instance, experiences twice larger phase changes compared to a wave backscattered by a scatterer located at depth of 5 cm in a homogeneous medium. On this account, soil moisture-induced InSAR phase change decreases by increasing the volume fraction and/or size of the scatterers. At the same time, however, the backscattered intensity increases as the volume fraction and/or size of the scatterers increases. This fact can be observed in our model's results shown in Fig. 2 and also in Figs. 5 and 6, which feature the comparison between real and modeled phase and intensity changes. It can be seen that the intensity is proportional to the volume geometric cross section whereas the phase change is inversely proportional to it. In other words, pixels with smaller volume geometric cross section are associated with larger soil moisture-induced phase changes and smaller intensities. Theoretically, a pixel can take large phases (e.g., 2 rad. and even larger); however, in practice, such pixels are difficult to study since the intensity gets closer to the noise equivalent

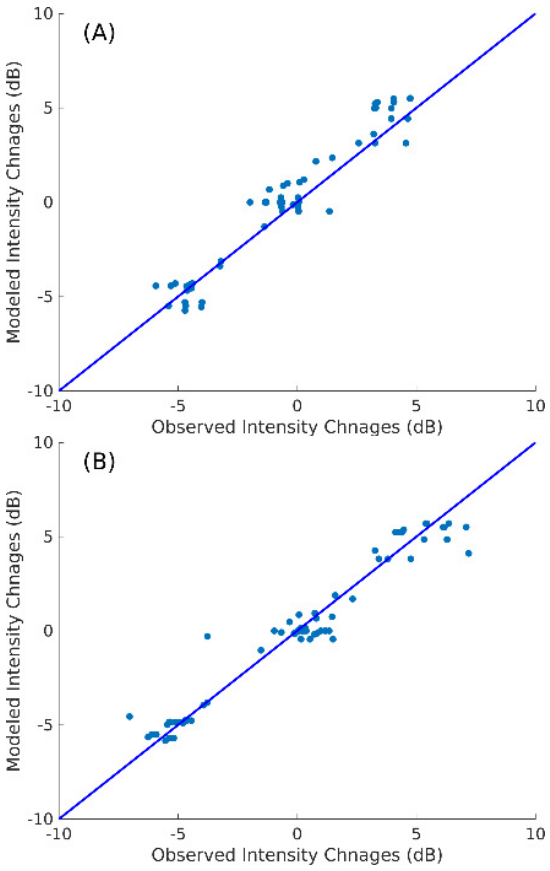

Fig. 7. Modeled and observed SAR intensity changes.

signal zero (NESZ). Therefore, the largest detectable soil moisture-induced phase changes are relevant to NESZ of the data.

Three measurements exhibit very high values on intensity plots (Fig. 6), indicating a strong change in the backscattering property of the soil. The observed out-of-range values (Fig. 6) are so high that even fully saturated soil could not generate such a strong backscattering. Therefore, the mechanism that leads to the high values of intensity could not be elucidated considering soil moisture changes solely. Instead, we attribute this to the change in the structure of soil due to freezing. The weather record over the study area indicates that the soil temperatures of the three measurements are below 0 °C. The dielectric constant of ice, which is about 3.2, is very close to the dielectric constant of soil particles. When soil freezes, the pore ice bonds soil particle together, resulting in a larger almost homogenous scatterer. The change in the structure of the soil due to freezing decorrelates the backscattered signals [26], leading to low coherence between frozen and nonfrozen soils. In this case where the coherence is low, intensity changes can be potentially used for analyzing the radar responses of the frozen soil. However, we do not cover this issue in this study as it is beyond the scope of this research.

VI. Conclusion

Unlike previous models, which are only applicable for either intensity or phase estimations, our volume scattering model successfully estimates SAR intensity changes as well as InSAR phase changes. Also, while previous interferometric models provide phase changes due to soil moisture changes, they do not take into account the structure of the soil, i.e., soil particle size and distribution. The model introduced in this article models the soil as a discrete dielectric constant medium with larger scatterers embedded within a finer grain background of soil. It takes into account the scatterers' sizes and their volumetric fraction. This may open a new window in the study of soil structure using SAR and InSAR methods.

The volume scattering models so far have been used along with surface models to estimate soil moisture-induced SAR intensity changes. Based on this hypothesis, the negative slope on intensity curves is attributed to volume scattering, which decreases by increasing the soil moisture. The volume scattering model provided in this article, however, is successful in estimating the SAR intensity changes.

The model in this article predicts the reverse relationship between soil moisture changes and SAR intensity changes for small soil moisture values. We attribute this to the difference between the dielectric constants of dense point scatterers and porous dry background.

The previous models lead to nonzero phase triplets for single-focused pixels, which is zero in real world and also in our model. This is because the models do not generate SAR images and instead they apply a cross correlation to estimate the phase changes from modeled pixels.

Acknowledgment

ALOS PALSAR data have been used to generate interferograms and phase triplets.

References

[1] D. Massonnet and K. L. Feigl, "Radar interferometry and its application to changes in the Earth's surface," *Rev. Geophys.*, vol. 36, no. 4, pp. 441–500, Nov. 1998.

[2] R. Bürgmann, P. A. Rosen, and E. J. Fielding, "Synthetic aperture radar interferometry to measure Earth's surface topography and its deformation," *Annu. Rev. Earth Planet. Sci.*, vol. 28, no. 1, pp. 169–209, May 2000.

[3] Z. Lu and D. Dzurisin, "InSAR imaging of Aleutian volcanoes: Monitoring a volcanic arc from space," in *Geophysical Sciences*. Chichester, U.K.: Springer, 2014, p. 390.

[4] Y. Eshqi Molan, J.-W. Kim, Z. Lu, B. Wylie, and Z. Zhu, "Modeling wildfire-induced permafrost deformation in an alaskan boreal forest using InSAR observations," *Remote Sens.*, vol. 10, no. 3, p. 405, Mar. 2018.

[5] A. Ferretti, C. Prati, and F. Rocca, "Permanent scatterers in SAR interferometry," *IEEE Trans. Geosci. Remote Sens.*, vol. 39, no. 1, pp. 8–20, Jan. 2001.

[6] Z. Lu and D. J. Meyer, "Study of high SAR backscattering caused by an increase of soil moisture over a sparsely vegetated area: Implications for characteristics of backscattering," *Int. J. Remote Sens.*, vol. 23, no. 6, pp. 1063–1074, Jan. 2002.

[7] M. Nolan, D. Fatland, and L. Hinzman, "Dinsar measurement of soil moisture," *IEEE Trans. Geosci. Remote Sens.*, vol. 41, no. 12, pp. 2802–2813, Dec. 2003.

[8] B. Barrett, "The use of C- and L-band repeat-pass interferometric SAR coherence for soil moisture change detection in vegetated areas," *Open Remote Sens. J.*, vol. 5, no. 1, pp. 37–53, Jun. 2012.

[9] S. Zwieback, S. Hensley, and I. Hajnsek, "Assessment of soil moisture effects on L-band radar interferometry," *Remote Sens. Environ.*, vol. 164, pp. 77–89, Jul. 2015, doi: 10.1016/j.rse.2015.04.012.

[10] F. De Zan, A. Parizzi, P. Prats-Iraola, and P. Lopez-Dekker, "A SAR interferometric model for soil moisture," *IEEE Trans. Geosci. Remote Sens.*, vol. 52, no. 1, pp. 418–425, Jan. 2014.

[11] S. Hensley *et al.*, "Effect of Soil Moisture on polarimetric-interferometric repeat pass observations by UAVSAR during 2010 Canadian Soil Moisture campaign," in *Proc. IEEE Int. Geosci. Remote Sens. Symp.*, Jul. 2011, pp. 1063–1066.

[12] A. Hooper, D. Bekaert, K. Spaans, and M. Arikan, "Recent advances in SAR interferometry time series analysis for measuring crustal deformation," *Tectonophysics*, vols. 514–517, pp. 1–13, Jan. 2012.

[13] R. F. Hanssen, *Radar Inteferometry: Data Interpretation and Error Analysis*. Norwell, MA, USA: Kluwer, 2001.

[14] A. K. Gabriel, R. M. Goldstein, and H. A. Zebker, "Mapping small elevation changes over large areas: Differential radar interferometry," *J. Geophys. Res.*, vol. 94, no. B7, pp. 9183–9191, Feb. 2008.

[15] M. Cardinali, F. Ardizzone, M. Galli, F. Guzzetti, and P. Reichenbach, "Landslides triggered by rapid snow melting, the December 1996-Jan. 1997 event in Central Italy," in *Proc. EGS Plinius Conf.*, Cosenza, Italy, 2000, pp. 439–448.

[16] D. A. Robinson *et al.*, "soil moisture measurement for ecological and hydrological watershed-scale observatories: A review," *Vadose Zone J.*, vol. 7, no. 1, pp. 358–389, Feb. 2008.

[17] M. Hirschi, P. Viterbo, and S. Seneviratne, "Basin-scale water balance estimates of terrestrial water storage variations from ECMWF operational forecast analysis," *Geophys. Res. Lett.*, vol. 33, L21401, 2006.

[18] W.-L. Liang, F.-X. Hung, M.-C. Chan, and T.-H. Lu, "Spatial structure of surface soil water content in a natural forested headwater catchment with a subtropical monsoon climate," *J. Hydrol.*, vol. 516, pp. 210–221, Aug. 2014.

[19] S. I. Seneviratne, P. Viterbo, D. Lüthi, and C. Schär, "Inferring changes in terrestrial water storage using ERA-40 reanalysis data: The mississippi river basin," *J. Climate*, vol. 17, no. 11, pp. 2039–2057, Jun. 2004.

[20] T. Zhang, Q. Zeng, Y. Li, and Y. Xiang, "Study on relation between InSAR coherence and soil moisture," in *Proc. ISPRS Congr.*, vol. 37, 2008, pp. 131–134.

[21] I. Hajnsek and P. Prats, "Soil moisture estimation in time with D-InSAR," in *Proc. IEEE Int. Geosci. Remote Sens. Symp. (IGARSS)*, Jul. 2008, pp. 546–549.

[22] G. Nesti, D. Tarchi, and J.-P. Rudant, "Decorrelation of backscattered signal due to soil moisture changes," in *Proc. Int. Geosci. Remote Sens. Symp.*, vol. 3, Jul. 1995, pp. 2026–2028.

[23] G. Nesti *et al.*, "Phase shift and decorrelation of radar signal related to soil moisture changes," in *Proc. 2nd ESA Int. Workshop Retr. Bio-Geo-Phys. Parameter SAR Data Land Appl.*, 1998, pp. 423–430.

[24] J.-P. Rudant, A. Bedidi, R. Calonne, D. Massonnet, G. Nesti, and D. Tarchi, "Laboratory experiment for the interpretation of phase shift in SAR interferograms,"in *Proc. Fringe*, 1996, pp. 83–86.

[25] K. Morrison, J. C. Bennett, M. Nolan, and R. Menon, "Laboratory measurement of the DInSAR response to spatiotemporal variations in soil moisture," *IEEE Trans. Geosci. Remote Sens.*, vol. 49, no. 10, pp. 3815–3823, Oct. 2011.

[26] Y. Eshqi Molan, J.-W. Kim, Z. Lu, and P. Agram, "L-band temporal coherence assessment and modeling using amplitude and snow depth over interior Alaska," *Remote Sens.*, vol. 10, no. 1, p. 150, Jan. 2018.

[27] A. Fung, Z. Li, and K. Chen, "Backscattering from a randomly rough dielectric surface," *IEEE Trans. Geosci. Remote Sens.*, vol. 30, no. 2, pp. 356–369, Mar. 1992.

[28] Z. Su, P. A. Troch, and F. P. De Troch, "Remote sensing of bare surface soil moisture using EMAC/ESAR data," *Int. J. Remote Sens.*, vol. 18, no. 10, pp. 2105–2124, Jul. 1997.

[29] N. Baghdadi and M. Zribi, "Evaluation of radar backscatter models IEM, OH and Dubois using experimental observations," *Int. J. Remote Sens.*, vol. 27, no. 18, pp. 3831–3852, Sep. 2006.

[30] E. Altese, O. Bolognani, M. Mancini, and P. A. Troch, "Retrieving soil moisture over bare soil from ERS 1 synthetic aperture radar data: Sensitivity analysis based on a theoretical surface scattering model and field data," *Water Resour. Res.*, vol. 32, no. 3, pp. 653–661, Mar. 1996.

[31] B. Barrett, E. Dwyer, and P. Whelan, "Soil moisture retrieval from active spaceborne microwave observations: An evaluation of current techniques," *Remote Sens.*, vol. 1, no. 3, pp. 210–242, Jul. 2009.

[32] P.-W. Liu, J. Judge, R. D. Deroo, A. W. England, T. Bongiovanni, and A. Luke, "Dominant backscattering mechanisms at L-band during dynamic soil moisture conditions for sandy soils," *Remote Sens. Environ.*, vol. 178, pp. 104–112, Jun. 2016.

[33] S. Zwieback, I. Hajnsek, A. Edwards-Smith, and K. Morrison, "Depth-resolved backscatter and differential interferometric radar imaging of soil moisture profiles: Observations and models of subsurface volume scattering," *IEEE J. Sel. Topics Appl. Earth Observ. Remote Sens.*, vol. 10, no. 7, pp. 3281–3296, Jul. 2017.

[34] L. Tsang, J. A. Kong, and K.-H. Ding, *Scattering of Electromagnetic Waves: Theories and Applications*. New York, NY, USA: Wiley, 2000, pp. 9–10.

[35] F. Ulaby, R. Moore, and A. Fung, *Microwave Remote Sensing: Active and Passive*, vol. 1. Boston, MA, USA: Artech House, 1981, pp. 334–335.

[36] C. Mätzler, "Improved Born approximation for scattering of radiation in a granular medium," *J. Appl. Phys.*, vol. 83, no. 11, pp. 6111–6117, Jun. 1998.

[37] Y. Lei, P. Siqueira, and R. Treuhaft, "A dense medium electromagnetic scattering model for the InSAR correlation of snow," *Radio Sci.*, vol. 51, no. 5, pp. 461–480, May 2016, doi: 10.1002/2015rs005926.

[38] R. N. Treuhaft, S. N. Madsen, M. Moghaddam, and J. J. Van Zyl, "Vegetation characteristics and underlying topography from interferometric radar," *Radio Sci.*, vol. 31, no. 6, pp. 1449–1485, Nov. 1996.

[39] C. Mätzler. (2012). *MATLAB Functions for Mie Scattering and Absorption*. [Online]. Available: https://omlc.org/software/mie/maetzlermie/Maetzler2002.pdf

[40] C. F. Bohren and D. R. Huffman, *Absorption and Scattering of Light by Small Particles*. New York, NY, USA: Wiley, 1983.

[41] A. Fung, *Microwave Scattering and Emission Models and Their Applications*. Norwood, MA, USA: Artech House, 1994.

[42] F. Ulaby, R. Moore, and A. Fung, *Microwave remote sensing: Active and passive*, vol. 3. Boston, MA, USA: Artech House, 1986.

[43] M. Hallikainen, F. Ulaby, M. Dobson, M. El-rayes, and L.-K. Wu, "Microwave dielectric behavior of wet soil—Part 1: Empirical models and experimental observations," *IEEE Trans. Geosci. Remote Sens.*, vols. GE–23, no. 1, pp. 25–34, Jan. 1985.

[44] J. C. M. Garnett and J. Larmor, "Colours in metal glasses and in metallic films.," *Philos. Trans., Roy. Soc. London A* , vol. 73, nos. 488–496, pp. 443–445, Jul. 1904.

[45] A. Sihvola, "Electromagnetic mixing formulas and applications," in *IEEE Electromagnetic Waves Series* (Institution of Electrical Engineers), vol. 47. Hertfordshire, U.K.: Stevenage, 1999.

[46] Y. E. Molan, Z. Lu, and J.-W. Kim, "Influence of the statistical properties of phase and intensity on closure phase," *IEEE Trans. Geosci. Remote Sens.*, to be published.

Yusuf Eshqi Molan received the B.S. degree from Sahand University of Technology, Tabriz, Iran, in 2006, and the M.S. degree from Amirkabir University of Technology, Tehran, Iran, in 2008. He is currently pursuing the Ph.D. degree in geophysics with Southern Methodist University, Dallas, TX, USA.

In 2008, he joined Remote Sensing Group, Geological Survey of Iran, Tehran, Iran. He was a Lecturer with the Sahand University of Technology from 2010 to 2015. His research interests include the use of interferometric synthetic aperture radar (InSAR) for deformation mapping, and multi/hyper-spectral data processing and analysis. His main research focus is modeling the influence of soil moisture on InSAR measurements.

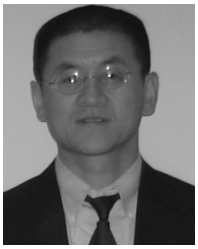

Zhong Lu (Senior Member, IEEE) received the B.S. and M.S. degrees from Peking University, Beijing, China, in 1989 and 1992, respectively, and the Ph.D. degree from the University of Alaska Fairbanks, Fairbanks, AK, USA, in 1996.

He was a Physical Scientist with United States Geological Survey, Vancouver, WA, USA, from 1997 to 2013. He is currently a Professor and Endowed Shuler-Foscue Chair with the Roy M. Huffington Department of Earth Sciences, Southern Methodist University, Dallas, TX, USA (www.smu.edu/dedman/lu). He has produced more than 200 peer-reviewed journal articles and book chapters focused on InSAR techniques and applications, and a book, *InSAR Imaging of Aleutian Volcanoes: Monitoring a Volcanic Arc from Space* (Springer, 2014). His research interests include technique developments of interferometric synthetic aperture radar (InSAR) processing and their applications to the study of volcano, landslide, and human-induced geohazards.

Dr. Lu is a member of NASA-India SAR (NISAR) Science Team, since 2012, Senior Associate Editor of the journals *Remote Sensing* and *Frontier in Earth Sciences*, and a member of editorial boards of the *International Journal of Image and Data Fusion,* and *Geomatics, Natural Hazards and Risk*.